Reduction of higher order mode generation in large scale gravitational wave interferometers by central heating residual aberration correction

R. A. Day,[1,*] G. Vajente,[2] M. Kasprzack,[1,3] and J. Marque[1]

[1]*European Gravitational Observatory (EGO), I-56021 Cascina, Pisa, Italy*
[2]*INFN, Sezione di Pisa, I-56127 Pisa, Italy*
[3]*LAL, Université Paris-Sud, IN2P3/CNRS, F-91898 Orsay, France*

(Received 12 March 2013; published 23 April 2013)

Imperfect cavity mirrors in the arms of an interferometric gravitational-wave (GW) detector can result in the generation of unwanted higher order modes that are close to or at resonance in the cavity. This can lead to many undesirable effects such as increased round-trip losses or degraded contrast defect. Polishing mirrors to fulfill the requirements of 2nd generation GW interferometers is extremely challenging. For the use of LG33 modes in 3rd generation detectors it would be necessary to improve polishing by an order of magnitude. In this article we present a novel technique for the *in situ* correction of cavity mirror surface figures by central heating residual aberration correction. This system targets and corrects specific features of the mirror surface figure such as to reduce scattering from the fundamental cavity mode to specific higher order modes by more than an order of magnitude. We demonstrate, by simulation, the feasibility of such a system and give examples of its application to 2nd and 3rd generation GW interferometers.

DOI: 10.1103/PhysRevD.87.082003 PACS numbers: 04.80.Nn, 07.60.Ly, 95.55.Ym

I. INTRODUCTION

Gravitational wave (GW) interferometers comprise the longest optical cavities in the world. These instruments, LIGO [1], Virgo [2], GEO600 [3] and TAMA300 [4], are designed to be sensitive enough to detect the differential displacement, induced by GW radiation, using a modified Michelson interferometer [5]. As an example, a schematic diagram of Virgo is shown in Fig. 1. A 3 km cavity is formed in each arm, made up of an input mirror and an end mirror of diameter 350 mm, in order to increase the lifetime of the photons in the arms thereby increasing the sensitivity to length changes. The GW signal is measured on the dark port of the interferometer. In order to further increase the power in the arm cavities, and hence increase the sensitivity, the light going back towards the laser is recycled by adding an additional mirror called the power recycling mirror. This mirror creates an additional cavity known as the recycling cavity. The world's GW experiments are currently building and commissioning the second generation GW interferometers which should be operational in 2015.

The guarantee of obtaining the design sensitivity for such an instrument relies heavily upon the near perfect destructive interference, at the dark port, of the two beams reflected from the arm cavities. However, these beams are degraded by the surface quality of the cavity mirrors which results in asymmetries and therefore unwanted power arriving at the dark port. The problem may be summarized as rough cavity mirrors scattering a small portion of the reflected beam into higher order modes (HOM's) of the Hermite Gauss basis. However, the mechanism of how this scattered light generates problems depends on the spatial frequency of the mirror roughness [6]. High spatial frequency roughness scatters the light at large angles. This is lost immediately from the cavity and therefore causes clipping losses which in turn reduces the cavity gain. Low spatial frequencies correspond to low order optical aberrations such as focus, astigmatism and coma. If these aberrations scatter light into HOM's that are close to or at resonance in the cavity then these unwanted modes will be amplified, effectively resulting in distortion of the cavity mode. Then finally we have the medium spatial frequency roughness. In this region light will again be scattered into HOM's that could be close to or at resonance.

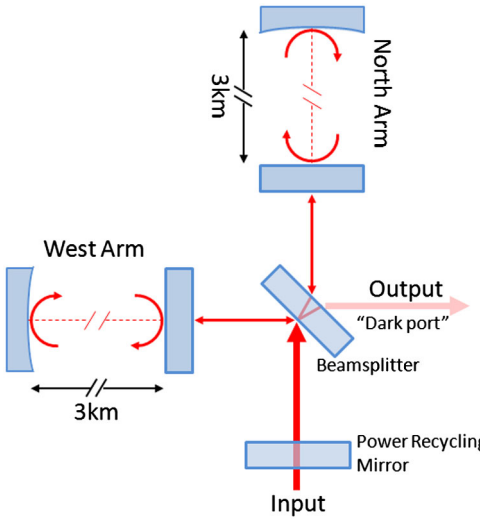

FIG. 1 (color online). Schematic optical design of Virgo.

*Corresponding author.
richard.day@ego-gw.it

However, in addition, the generated modes may be larger than the cavity optics. Therefore the amplification of these HOM's can substantially increase the clipping losses.

During the commissioning of Virgo+ and the third scientific run carried out from July to October 2010, many of the problems associated with imperfect cavity mirrors were observed experimentally [7]; the high spatial frequencies generated large clipping losses resulting in large loss asymmetries. The errors in radii of curvature and astigmatism on the end mirrors created poor overlapping of the beams at the dark port. The medium spatial frequencies resulted in the excitation of the near resonance transverse electro-magnetic mode of order 5 (TEM5) which increased clipping losses and spoilt the error signals, on the dark port, used for the alignment system. The problems encountered with Virgo+ were taken into account when defining the polishing requirements for the mirrors of the second generation GW interferometer Advanced Virgo (AdV) which is planned to be operational in 2015 [8]. State-of-the-art techniques will be used, such as ion-beam figuring and corrective coating [9] in order to ensure the highest quality surface possible using existing technologies. The expected RMS roughness for Advanced Virgo mirrors is of 0.5 nm on the central diameter of 150 mm, which is almost an order of magnitude better than that achieved for Virgo +. However, the fundamental limitation for these advanced polishing techniques lies in the metrology. We find ourselves polishing close to the limit of what is measurable. Even the geometry of the mirror mount and the environmental conditions can effect the final measurement. In addition the mirror will deform when suspended in the interferometer. Ultimately the final validation of such a process will be the *in situ* measurements made in the complete AdV installation. The goal for AdV is to have a sensitivity 10 times higher than that of Virgo +. The risks associated with imperfect cavity mirrors is high and so a method of correcting the mirrors *in situ* would appear desirable. In the final Virgo Scientific Run from June to September 2011, the central heating radius of curvature correction (CHRoCC) was used to change the radii of curvature of the end mirrors [7]. This made it possible to improve the overlapping at the dark port. In AdV there will be ring heaters [8] which will also be used to modify the radii of curvature of the mirrors. However, in Virgo +, one of the main problems was the resonance of the TEM5 mode. The CHRoCC was used to modify the radii of curvature of both end mirrors such that the TEM5 mode was no longer resonant. In AdV this is a technique that we will not be able to use. Changing the radius of curvature from that of the design would decrease the beam radius on one of the two cavity mirrors thereby increasing the coating thermal noise [10]. Therefore if we are to reduce the presence of HOM's in AdV we must minimize the scattering of light into the HOM's that are near resonance in the cavity.

For third generation detectors it has been proposed [11] to use a Laguerre Gauss 33 (LG33) mode instead of the TEM00 mode used in first and second generation detectors. This would have the advantage of decreasing considerably the coating thermal noise, thereby increasing the sensitivity of the detector [12]. However, it has been found, by simulation [13,14] and experimentally [15], that the use of current polishing technology is insufficient to obtain the required quality of cavity mode. This problem arises from the fact that, as well as the LG33 mode, there are also nine other exactly degenerate modes. Therefore any scattering from the LG33 mode to any of these other degenerate modes has a catastrophic effect on the mode quality. It is estimated that the required RMS roughness would be about 10^{-2} nm [13], which is an order of magnitude lower than what is possible with current polishing technology. Analytical studies [14] have shown that, in order to reduce the scattering into the other degenerate modes, it is sufficient to minimize certain types of aberrations, such as astigmatism, during

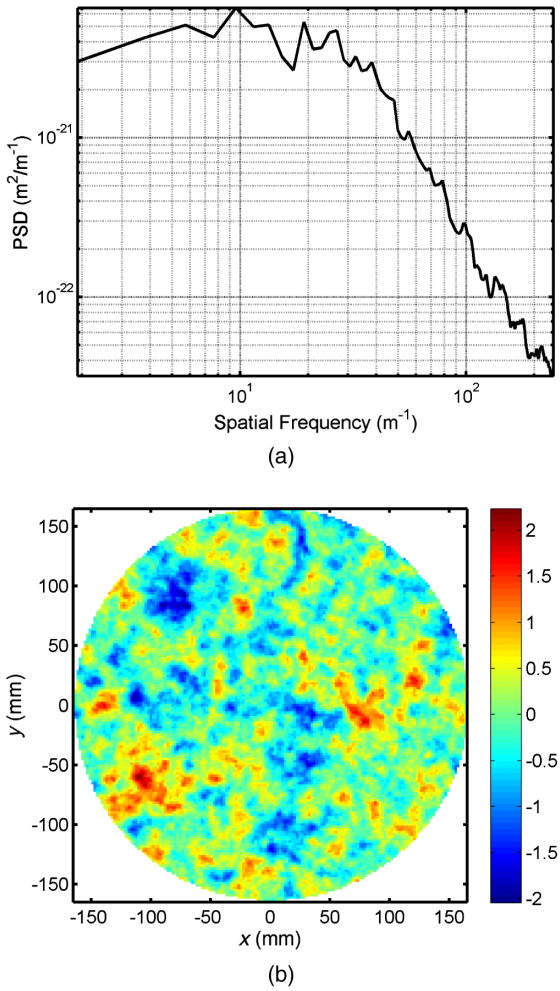

FIG. 2 (color online). (a) Typical power spectral density (PSD) of AdV grade mirrors. (b) Example mirror map randomly generated from PSD. Color scale in nm.

the polishing process rather than reducing the overall RMS. However the limitations of current metrology mean that this could not be achieved in practice.

The problems that we will encounter in AdV and in the possible use of LG33 modes in third generation detectors are similar. We need to suppress the scattering of light from the fundamental mode to certain other modes. In this paper we present a conceptual design for such a device. The central heating residual aberration correction (CHRAC) is an extension of the work carried out on the CHRoCC. A heat pattern is projected onto the high reflectivity coating of the cavity mirrors. The heating creates local deformation of the surface of the mirror thereby changing its shape. We may therefore adjust the spatial distribution of the heat pattern such as to remove specific aberrations of the mirror which will minimize scattering into certain HOM's. We would use the interferometer signals in order to optimise the correction. As we are targeting just certain aberrations for which the amplitude is extremely small, the amount of heating power required will be minimal. In this paper we will focus in particular on the case of AdV, but we will then discuss briefly how the same concept could also be used in the case of LG33 modes.

II. IMPERFECT MIRRORS IN ADVANCED VIRGO

The 3 km arm cavities for AdV have a bi-concave geometry. The input and end mirror radii of curvature are, respectively, 1420 and 1683 m [8]. The beam radii at the input and end mirrors are, respectively, 48.7 and 58 mm. This near concentric configuration is chosen such as to maximize the beam radius on the mirrors which, in turn, minimizes the relative contribution of mirror coating thermal noise. The finesse of the cavity is of 450. During the design stage of AdV, FFT simulations were used intensively to set the polishing requirements for the cavity mirrors. In particular, studies were focused on minimizing the total round-trip losses to less than 75 ppm, which is a critical parameter for reaching the required stored power in the arms. Figure 2(a) shows the specified power spectral density (PSD) for the cavity mirrors which corresponds to a total RMS roughness of 0.5 nm. Figure 2(b) shows a mirror map randomly generated from such a PSD.

This PSD was used to generate many random maps. These random maps were used on the cavity mirrors to simulate the round trip losses in the AdV arm cavities. It was therefore shown statistically that mirrors meeting the specified PSD would meet the round-trip loss requirements. In Fig. 3 we show the result of a typical FFT simulation of the arm cavity using the simulator *fast Fourier transform optical simulation of gravitational wave interferometers* (FOG) [16].

On both mirrors of the cavity we have placed a randomly generated mirror map. Throughout this article we use the same pair of maps. However, it was verified that the results obtained using these maps are representative of what is obtained using other random maps. In this example we simulate the cavity while changing the radius of curvature of the end mirror from the design value. The nominal value for the radius of curvature is situated directly between HOM degeneracies of order 8 and 9. In Fig. 3(a) we show the 8th and 9th HOM content reflected by the cavity for an input power of 1 W. We see clearly that the HOM content increases when the HOM in question is close to resonance. The more light scattered by the mirrors into this HOM, the greater its content will be. As this HOM will be uncorrelated with the other arm cavity, it will be found directly on the dark port of the interferometer. Figure 3(b) shows the calculated round-trip losses of the cavity. We see that the presence of these HOM's has a detrimental effect on the round-trip losses due to these modes being larger than the cavity mirrors. We may therefore conclude that, at the design radius of curvature, we have round-trip losses that are not only due to large angle scattering, but also due to the HOM 8 and 9 content in the cavity mode. This leads

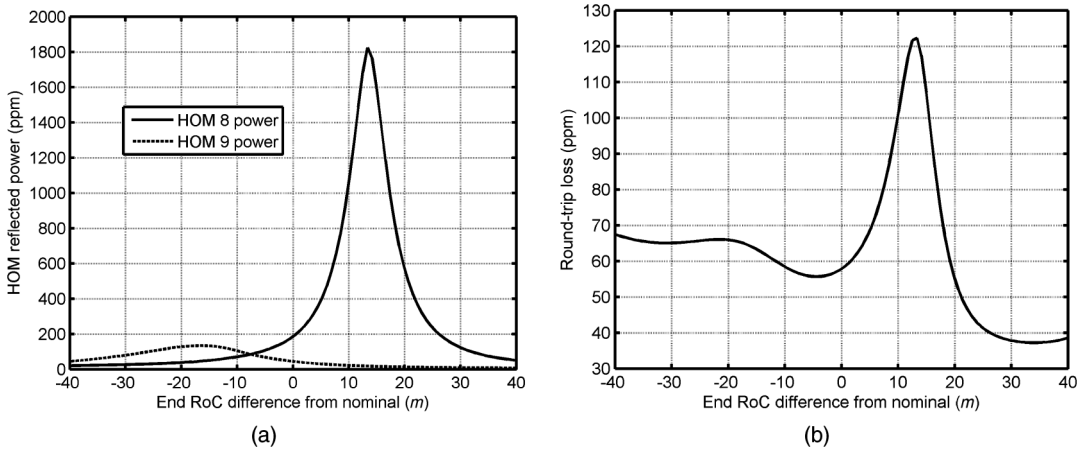

FIG. 3. (a) Higher order modes 8 and 9 content in reflected beam for different end mirror radii of curvature. (b) Round-trip losses. Peaks in round-trip losses correspond to peaks in HOM content in the cavity mode.

to the need for a strong requirement on the absolute radius of curvature of the cavity mirrors in order to minimize round-trip losses. We see that increasing the nominal radius of curvature by 30 m would greatly improve the round-trip losses. However, this would also decrease the beam radius on the end mirror thereby increasing the coating thermal noise.

III. SELECTIVE SUPPRESSION OF HIGH ORDER MODES

Our objective is to minimize the HOM 8 and 9 content in the cavity mode by modifying the surface figure of the cavity mirrors. Therefore the first step is to determine what components of the mirror surface figure scatter light from the fundamental mode into these HOM's. When we consider a mirror metrology map $M_0(x, y)$, where x and y are transverse coordinates, the field E_r reflected off the mirror is given by

$$E_r(x, y) = ie^{-2ikM_0(x,y)}E_0(x, y), \tag{1}$$

where E_0 is the incident fundamental mode field, $k = 2\pi/\lambda$ and λ is the wavelength of the field.

This reflected field is then decomposed into the Hermite-Gaussian modes using the ideal cavity mode parameters as the basis. We then set to zero the coefficients corresponding to the HOM's that we wish to suppress; in this case we wish to remove the modes 8 and 9. With the desired coefficients set to zero, we then recompose the field with the remaining coefficients which yields the modified field E_b. The ideal map that would produce exactly this field (given by the ratio E_b/E_r) is not physically feasible, since it involves also a modification of the field amplitude, or in other words it is not possible to obtain it without changing also the mirror reflectivity.

We therefore consider the effect of a correction map $M_c(x, y)$ added to the mirror and search for the one that provides the reflected field closest to the desired one. This is obtained by minimization of the following merit function:

$$e = \iint |E_b(x, y) - ie^{-2ik(M_c(x,y)+M_0(x,y))}E_0(x, y)|^2 dxdy. \tag{2}$$

The minimum can be found analytically using standard variational techniques. However, we prefer to adopt a different approach. Following what was done in Ref. [14] to analyze the surface map, we expand the correction in terms of Zernike polynomials:

$$M_c(x, y) = \sum_{n,m} \alpha_{n,m} Z_n^m(x, y). \tag{3}$$

The main index n is allowed to range from 0 to a maximum value N. The secondary index can take all even spaced values from $-n$ to n. In this way the minimization problem can be solved with standard numerical algorithms. The advantage of this approach, with respect to the completely analytical one, is that it allows us to retain a better control of the correction spatial frequencies, through the choice of the maximum Zernike order N.

In Fig. 4 we show an example of the resulting maps from such a calculation. Figure 4(a) is the original metrology map on the cavity input mirror and corresponds to M_0. Figure 4(b) is the optimal correction to cancel the 8th and 9th order HOM's, where Zernikes up to order 40 were used. Figure 4(c) is the sum of the two maps. It is interesting to note that the corrected mirror map appears, at first sight, to be almost identical to the original; the RMS of the corrected map is of 0.4 nm while the original has an RMS of 0.5 nm. The RMS of the correction to be made to the map is of 0.3 nm. The RMS is calculated inside a diameter of 150 mm which is roughly three times the beam radius.

We also see in Fig. 4(b) that there appears to be a characteristic spatial frequency in the pattern. To better understand this point, we repeated the corrective map computation for the end mirror, where the beam size is

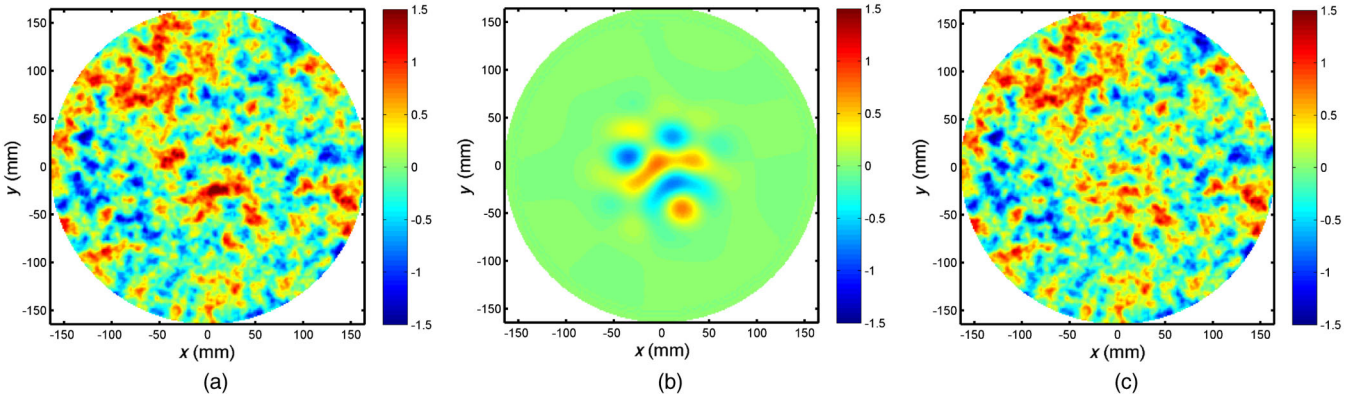

FIG. 4 (color online). Suppression of scattering into HOM 8 and 9 by correcting input mirror map. (a) Original randomly generated mirror map. (b) Optimal correction to cancel the 8th and 9th order HOM's, where Zernikes up to order 40 were used. (c) Corrected mirror map. Color scale in nm.

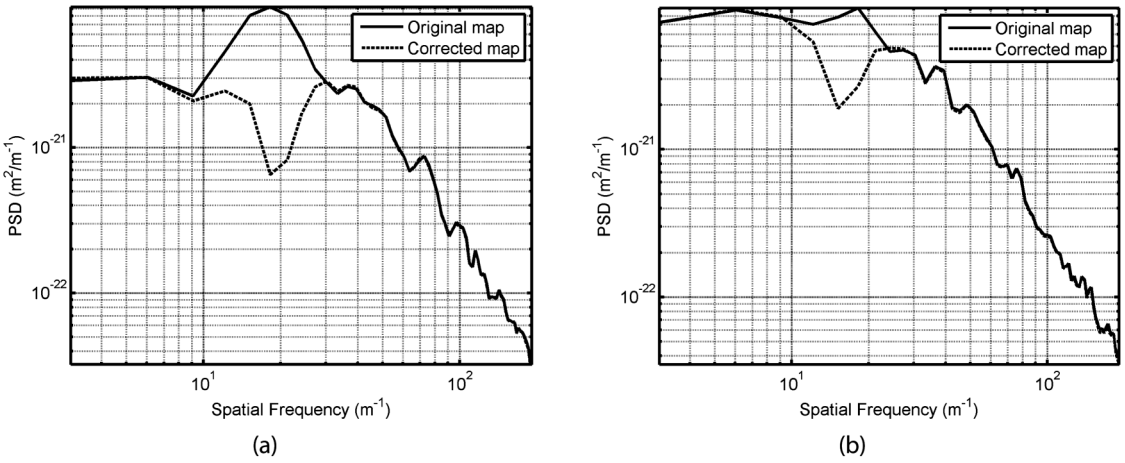

FIG. 5. Comparison of mirror map PSD before and after correction for input and end mirrors. (a) Input mirror map. Dip in spatial frequency at 20 m^{-1}. (b) End mirror map. Dip in spatial frequency at 16 m^{-1}.

slightly different. In Fig. 5 we compare the PSD of the original map with the PSD's of the corrected maps on the input mirror and on the end mirror. We see that there is a trough in the PSD's at 20 m^{-1} and 16 m^{-1} for the input and end mirrors, respectively. In both cases, this frequency is directly correlated to the characteristic spatial frequency of the amplitude distribution of the 8th and 9th HOM's. This spatial frequency at the end mirror is lower due to the base mode being larger [6].

In order to validate this method for reducing HOM content in cavities we will redo the simulation that gave the result in Fig. 3. However this time we will use corrected mirror maps that have had the HOM 8 and 9 scattering component removed. As the ideal cavity mode changes slightly with the radius of curvature of the end mirror, we must recalculate the modified map for each point of the plot. The result is shown in Fig. 6. We see that the modified maps have resulted in a notable reduction in the HOM content by a factor of greater than 20. In particular we see that even at the design radius of curvature, where we are seeking to avoid HOM degeneracy, the round-trip loss has been reduced by 40%. Even such a small reduction in clipping losses can have a profound effect on the interferometer efficiency and performance, as the power circulating inside the interferometer scales linearly with the round-trip losses. We may therefore conclude from this chapter that it is theoretically possible to identify and remove components of the mirror surface figure that scatter light from the fundamental mode into HOM's that are near resonance in an optical cavity.

IV. CHRAC PRINCIPLE

The method by which we propose to remove these surface figure components that scatter light into HOM's is by projecting a heat pattern that will locally deform the surface of the mirror. We refer to this technique as central heating residual aberration correction (CHRAC).

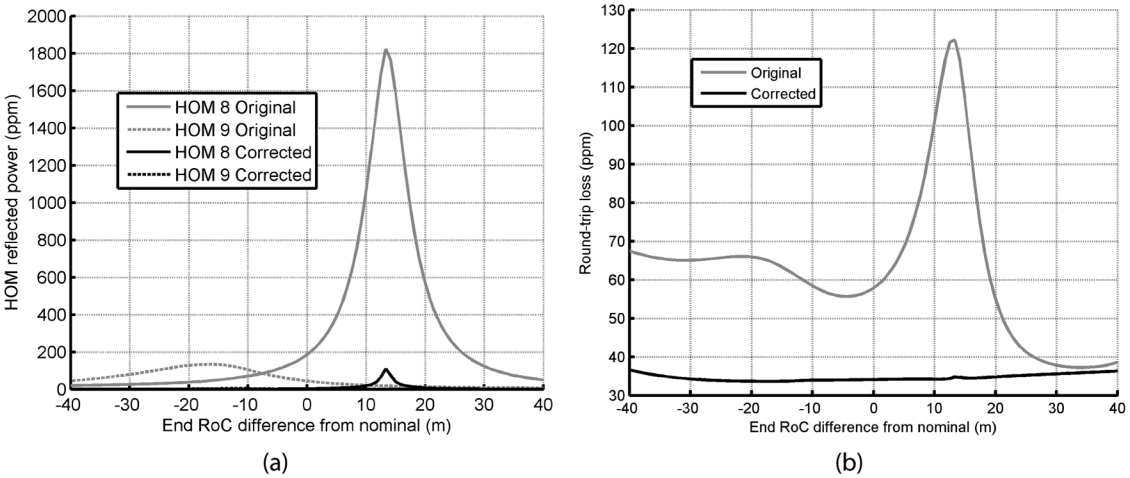

FIG. 6. Comparison of original and corrected mirror maps in arm cavity (a) Higher order mode 8 and 9 content in reflected beam for different end mirror radii of curvature. (b) Round-trip-losses.

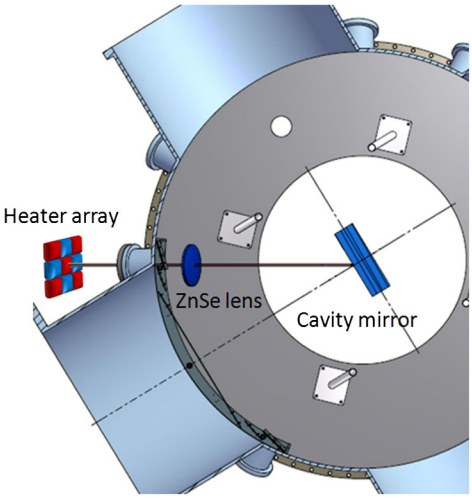

FIG. 7 (color online). Schematic design of CHRAC.

A conceptual schematic setup of a CHRAC system mounted on one of the core optics of AdV is shown in Fig. 7. The CHRAC consists of an array of Alumina ceramic heaters mounted outside of the mirror payload vacuum tower. Each heater element would have a surface area of about 1 cm^2 and would have a maximum working temperature of 1200 degrees Celsius. This heater array is imaged onto the high reflectivity surface of the cavity mirror using an in-vacuum Zinc Selenide lens of 200 mm diameter. As the cavity mirror surface is tilted with respect to the lens axis, the heater array is also tilted such that the image plane coincides with the cavity mirror surface at all points. In order to estimate the shape and intensity of the heat pattern projected onto the cavity mirror we use the standard ray tracing software *Zemax*. Figure 8 shows the simulated heat pattern incident on the high reflectivity surface of the cavity mirror when five pixels of the 3×3 array are switched on. The object-image magnification in this example is of 2.3. The elongated shape is due to the non-normal angle of incidence between the optical axis of the imaging lens and the cavity mirror surface, as was seen in Fig. 7. The non-square pattern is not in any way a problem, although it could be corrected by changing the shape and dimensions of the source heaters. Ideal blackbody heat sources emit with a Lambertian distribution, therefore the efficiency of the projection system is largely dependent on the numerical aperture of the optical system. In this example there is 6.4% of the emitted power which reaches the surface of the cavity mirror. In order to calculate the amount of power absorbed by the mirror substrate for a given heater temperature we must take into account the emission spectrum of an ideal black-body at a given temperature, the emissivity spectrum of the Alumina heater and the absorption spectrum of the fused silica mirror substrate. In Fig. 9 we see how these spectra are multiplied to yield the absorbed power calculated for a

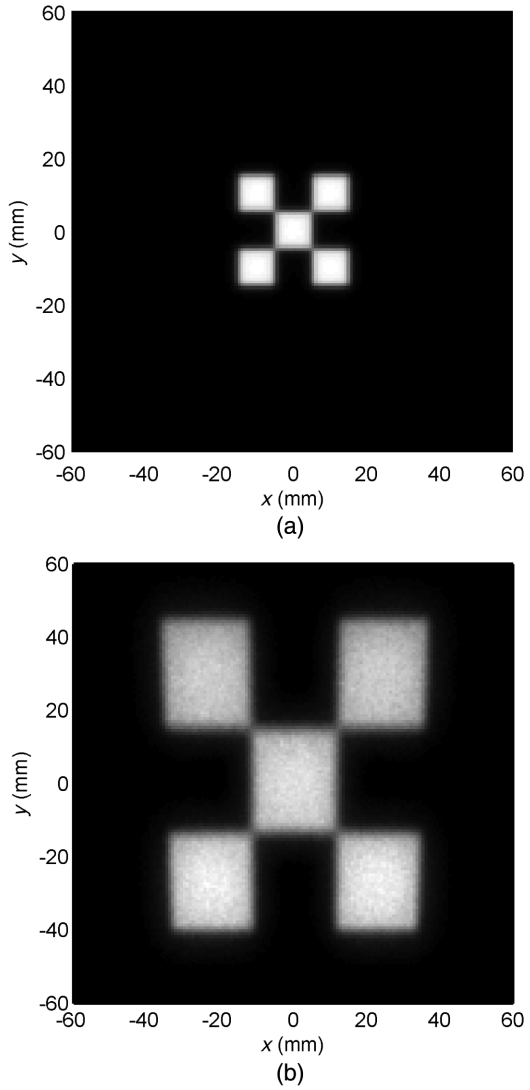

FIG. 8. Monte carlo simulation of infrared radiation emitted from a 3×3 array of black-body heat sources, for which 5 pixels are switched on. (a) Heat pattern directly after heater array (b) Heat pattern of the image projected onto the surface of the cavity mirror.

given heater temperature. Figure 10 plots the calculated intensity absorbed by the mirror substrate as a function of heater temperature. We may therefore conclude that, for the maximum heater working temperature of 1200 degrees Celsius, a maximum intensity of 52 mW/cm^2 can be absorbed by the mirror substrate.

We see from Fig. 5 that the correction map has spatial frequencies up to 30 and 24 m^{-1} for the input and end mirror, respectively. Considering the Nyquist theorem this means that the size of one heating element on the mirror must be no larger than 17 and 21 mm, respectively, in order to ensure optimal correction. In order to compensate for all scattering from the fundamental mode, the heating pattern must have a width of at least 3 times the beam radius incident on the mirror. We saw in Fig. 4(b) that this is

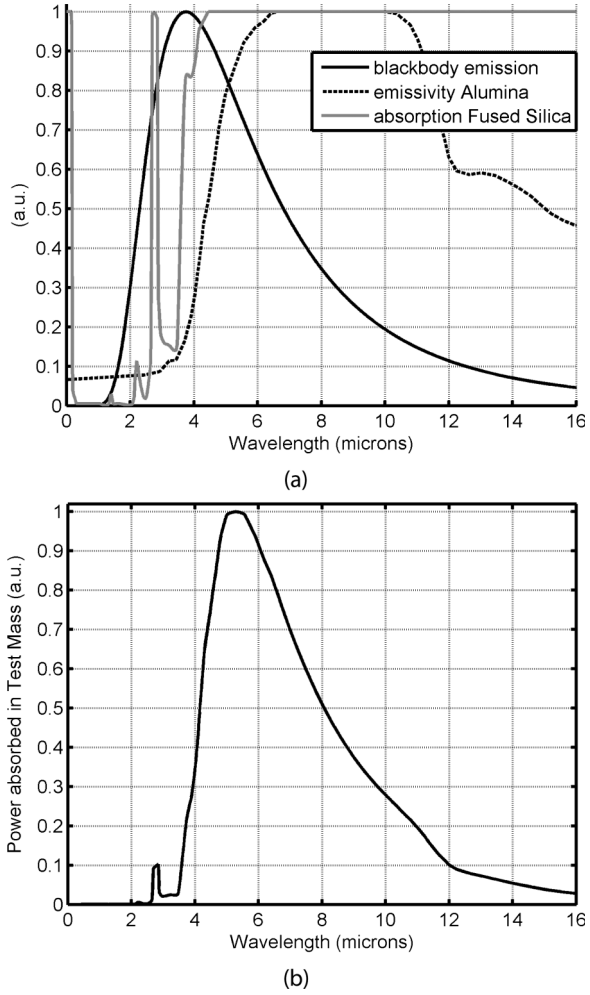

FIG. 9. Calculation used to estimate power absorbed in cavity mirror. (a) Spectrum plots for emissivity of alumina, absorption of cavity mirror substrate (fused silica) and blackbody emission for a blackbody temperature of 500 degrees C. (b) Product of three spectra in 9(a) resulting in spectrum of absorbed power for a heat source at 500 degrees C. Peak wavelength is just above 5 microns.

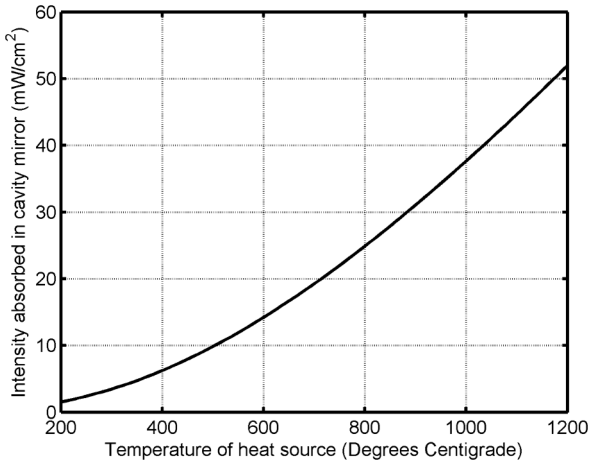

FIG. 10. Calculated intensity absorbed by the cavity mirror for a blackbody heater with varying temperature.

the region in which a correction is required. We may conclude that the heating array must have at least 9×9 elements. In the interests of simplicity, from here on we will consider that the heater elements are designed such that they project onto the cavity mirror an array of squares that are equal in size. In order to determine how the heat absorbed by the mirror deforms its surface we carry out finite element thermal simulations using *Ansys*. Figure 11 shows the results of such a simulation with just one heater switched on. The heater element projects a square having a dimension of 1×1 cm^2 on the mirror. The heater is operating at 500 degrees Celsius and the mirror is absorbing 10 mW. Figure 11(a) shows the temperature distribution at the surface of the mirror and Fig. 11(a) shows how the surface figure of the mirror has been modified due to

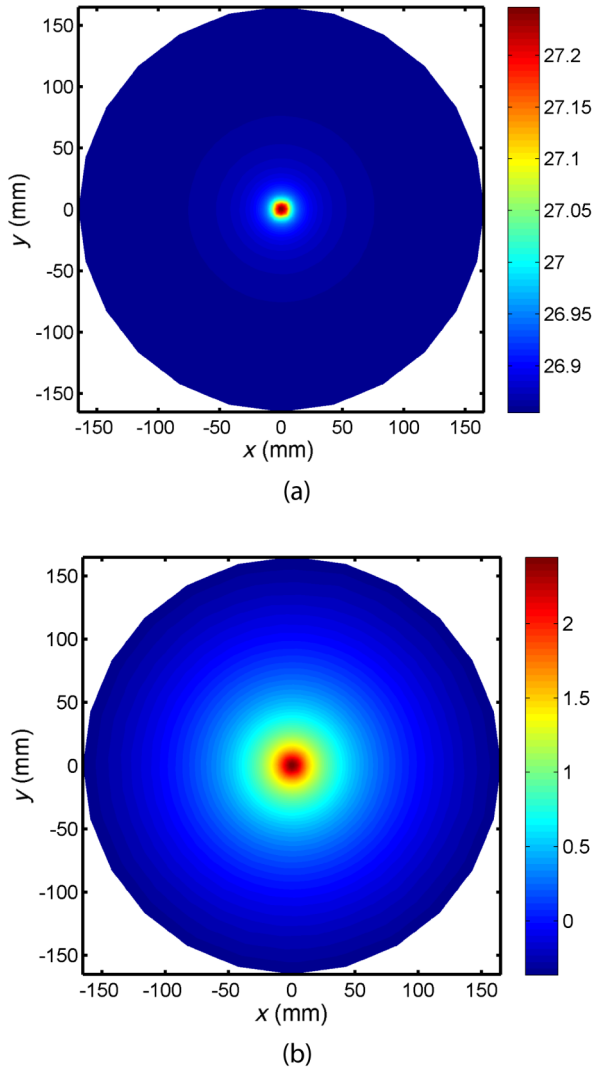

FIG. 11 (color online). Finite element simulation of a projected square of 1×1 cm^2 yielding an absorbed intensity of 10 mW/cm^2. (a) Mirror surface temperature distribution. Color scale in degrees Celsius. Ambient temperature of 26.85 degrees Celsius. (b) Change in surface figure. Color scale in nm.

thermo-elastic expansion. In the terminology of adaptive optics this figure is referred to as an *influence function* as it is the characteristic shape corresponding to the mirror response to the action of a single actuator. To a first order approximation, the mirror response is proportional to the power absorbed. We may therefore use the standard adaptive optics techniques to determine the heat pattern required to produce the desired correction of the mirror figure. The two-dimensional correction map is converted into vector format to give, $\mathbf{M}_T$, a $\mathrm{M} \times 1$ vector. This may be obtained by a linear sum of contributions from each actuator as

$$\mathbf{M}_T = \mathbf{BA}. \tag{4}$$

$\mathbf{B}$ is a $\mathrm{M} \times \mathrm{N}$ matrix known as the influence matrix. It contains the influence functions of all N actuators. $\mathbf{A}$ is a $\mathrm{N} \times 1$ matrix containing the coefficients of all the actuators. The actuators can deform the mirror surface in only one direction. $\mathbf{A}$ must therefore be positive. The actuator powers required to produce the correction map closest to the desired correction map are given by minimization of the function of merit:

$$\epsilon = \| \mathbf{M}_T - \mathbf{BA} \|_2^2 . \tag{5}$$

The method proposed in Ref. [17] takes advantage of the parabolic shape of the problem to solve equation (5) with boundary conditions. It allows to define a solution domain of positive power values smaller than 52 mW for 1 cm^2 actuators. The solution is the local minimum of the equation inside the restricted domain and then ensures the stability of the solution. In Fig. 12 we present the correction map obtained by such a method for a 15×15 array. Figure 12(a) shows the correction map that we wish to reproduce. Figure 12(b) shows the resulting heating pattern that we obtain from the minimisation algorithm. The total actuator power is of 615 mW and the peak actuator power is of 7 mW. Figure 12(c) shows the corresponding correction map obtained from the sum of

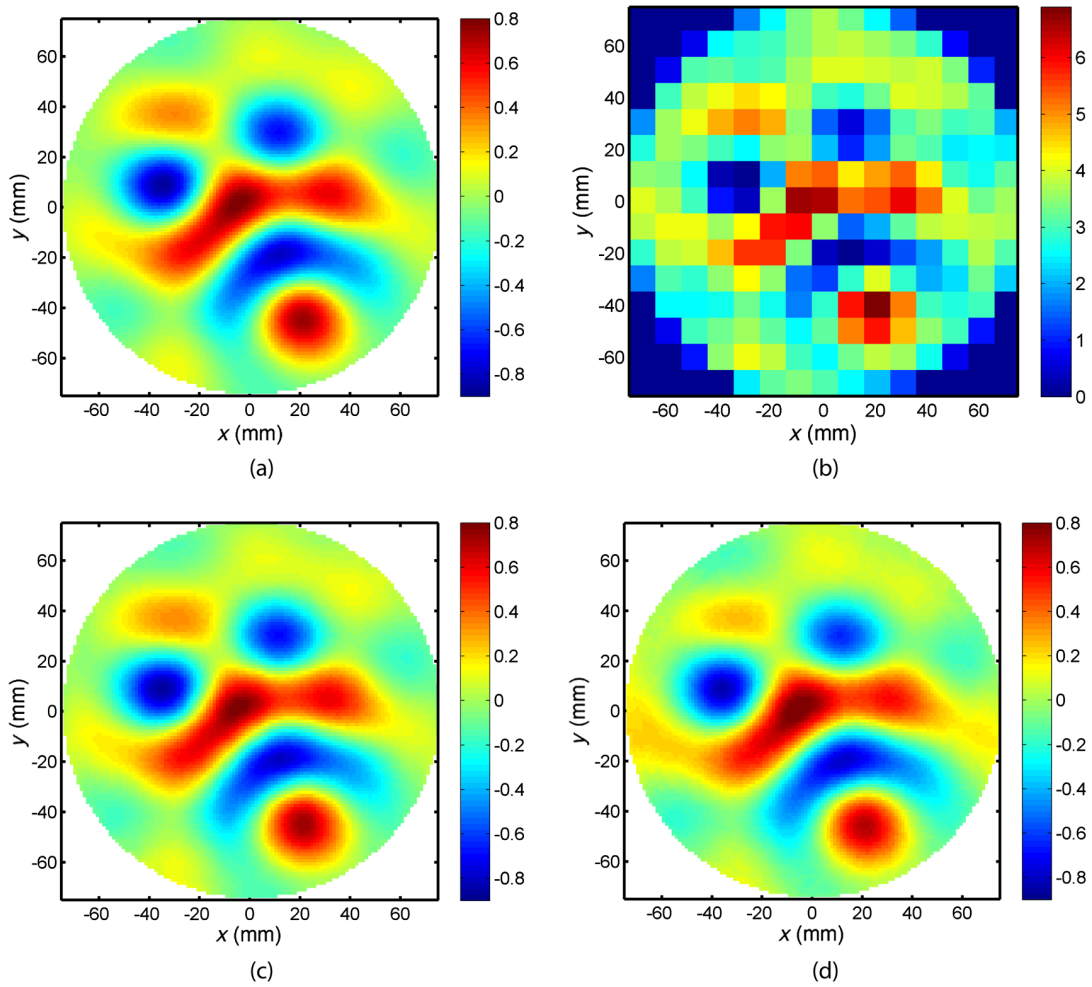

FIG. 12 (color online). Validation of adaptive optics approach to finding CHRAC actuator powers to correct mirror surface figure. (a) Target correction map to be generated by CHRAC. Color scale in nm. (b) Actuator power to be absorbed by mirror. Color scale in mW. (c) Reconstructed correction map from optical influence matrix and derived actuator powers. Color scale in nm. (d) Surface figure obtained using actuator powers of Fig. 12(b) in *Ansys* simulation. Color scale in nm.

TABLE I. Comparison of corrected map performance in terms of reduction of HOM 8 and 9 generation and reduction of round-trip losses.

Maps	HOM 8 reflected power (ppm)	HOM 9 reflected power (ppm)	Round-trip losses (ppm)
Original	186	44	58
Analytical correction	8	1	33
CHRAC correction	6	1	34

contributions from each actuator influence function. We validated this result by running the *Ansys* simulation using the heat pattern of Fig. 12(b) which gives the result in Fig. 12(d). The two results are almost identical. The slight difference that we see far from the center comes from the fact that the influence function of Fig. 11(b) was replicated and translated to construct more simply the optical influence matrix. Far from the center we therefore start seeing the second order effects of the off-axis influence functions. It should be noted that a focus of 6.5 μdpt has been removed from the result of Figs. 12(c) and 12(d). Indeed corrections using the CHRAC technique result unavoidably in unwanted focus. However, due to the low actuation powers it would be possible to compensate for this focus using the heating ring installed on the mirror payload. Another important technical detail is the use of the CHRAC on the input mirror of the cavity. As we saw in Fig. 1, the input mirror is also used in transmission. The CHRAC heating pattern will therefore generate substantial aberrations in the recycling cavity of the interferometer. It would therefore be necessary that the thermal compensation system [18], that is used to compensate aberrations in the recycling cavity, be capable of correcting these additional aberrations. With the extreme sensitivity of GW detectors to environmental noise we must also consider possible sources of noise due to the installation of the CHRAC system. Any fluctuations in the radiation intensity could result in thermo-optic noise [19] on the surface of the cavity mirror. The ceramic heater is a relatively quiet heat source due to its long thermal time constant. The contribution due to this noise source could be further minimized by using an extremely stable current source. Another possible source of noise is the air turbulence between the in-air heater array and the vacuum chamber view port. It would therefore be preferable to contain the heater array in a low-vacuum chamber. However, it should be noted that during the commissioning and scientific run with the installed CHRoCC [7], which is a similar device, no experimental evidence was found to suggest that it was affecting the sensitivity of Virgo +.

Finally in Table I we compare the performance of cavity mirrors corrected by the CHRAC system with that of the original mirrors and the analytically corrected mirrors using the design radii of curvature. We may conclude that the use of CHRAC to remove the surface figure component that scatters light into HOM's 8 and 9 yields a significant reduction in HOM content and hence round-trip losses.

V. MERIT FUNCTION OPTIMIZATION

The computation of the correction presented so far is based on the knowledge of the mirror surface map. This might not always be available and it might not have the required accuracy. It is therefore interesting to devise a completely adaptive optics system. For this goal, we require however an algorithm to extract the correct map from interferometric signals and images. It is clear that in the case of the full interferometer this is not a simple task due to the coupling of the different effects and the nonlinear nature of the cavity response. A detailed study of this procedure has been done and results will be reported in a dedicated paper. However, we hope to give a few pointers as to the approach that could be adopted.

We do not expect to be able to completely sense the amplitude and phase of the beam reflected by the cavities with sufficient accuracy. Therefore our adaptive optics system will need to implement a *wave-front-sensor-less* approach [20]. The spatial distribution of intensity at different ports of the interferometer, mainly at the anti-symmetric port, could be analyzed to extract an estimation of the mode content. These can then be used as error signals or merit functions for an optimization algorithm. In the worst case simply the total power reflected by the cavities or the power at the anti-symmetric port can be used as the quantity to be optimized.

Given the large number of actuation degrees of freedom involved in the CHRAC system, standard minimization searches would take too much time. We foresee to tackle this issue with two complementary approaches. First, the number of degrees of freedom could be reduced by finding appropriate basis functions for the CHRAC actuation. Second, an optimized blind search can be implemented using *stochastic parallel-gradient-descent* algorithms [21].

VI. APPLICATION TO LAGUERRE GAUSS MODES

We have therefore seen that, in the case of AdV, the CHRAC technique could be used to minimize scattering

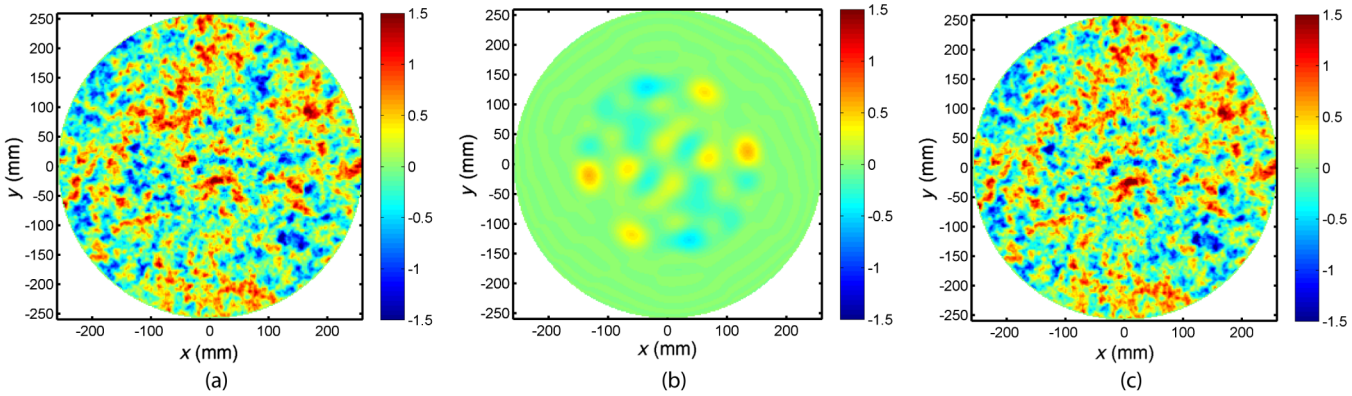

FIG. 13 (color online). Suppression of scattering of LG33 mode into other 9th order modes by correcting input mirror map. (a) Original randomly generated mirror map. (b) Optimal correction to cancel scattering into other 9th order modes. (c) Corrected mirror map. Color scale in nm.

into HOM's that are close to resonance in the arm cavity. In this section we will briefly discuss the application of the same technique to the problem of using LG33 modes in the arm cavity. As we mentioned previously the LG33 mode is part of a family of degenerate modes. As all of these modes are at resonance in the cavity, the scattering of the fundamental mode into these HOM's is particularly problematic. We use the same cavity geometry and 00 mode basis as before. As the LG33 mode is larger than the HG00 mode the mirror diameter is increased to 52 cm such that the round-trip clipping losses using perfect mirrors is less than 1 ppm. When we simulate the arm cavity with imperfect mirrors, as before, and use the LG33 as the fundamental mode, we find that the reflected beam has only 79.0% that remains in the fundamental mode which is unacceptable. We therefore use the same treatment as in Sec. III to determine a mirror map that has no components that scatter the LG33 mode into other 9th order modes. Figure 13(a) is the original metrology map on the cavity input mirror. Figure 13(b) is the correction map. Figure 13(c) is the corrected map. We see that the resulting correction map is very different to what we saw in the case of AdV in the previous sections. The RMS of the correction map is of 0.1 nm. As before we simulate the CHRAC heat pattern necessary to generate the same correction as Fig. 13(b). The LG33 mode covers a larger portion of the mirror than the Hermite Gauss mode, so we use square actuators that are 2×2 cm^2 at the surface of the mirror in a 20×20 configuration. The maximum actuator power is 5.5 mW and the total power is 590 mW. We now redo the simulation of the arm cavity, this time using corrected mirror maps that have had the 9th order scattering component removed. Figure 14 shows the intensity distribution of the reflected beam before [Fig. 14(a)] and after [Fig. 14(b)] correction. We now find that the LG33 content in the cavity mode has increased to 99.98% which may be considered an acceptable value for the correct functioning of the GW

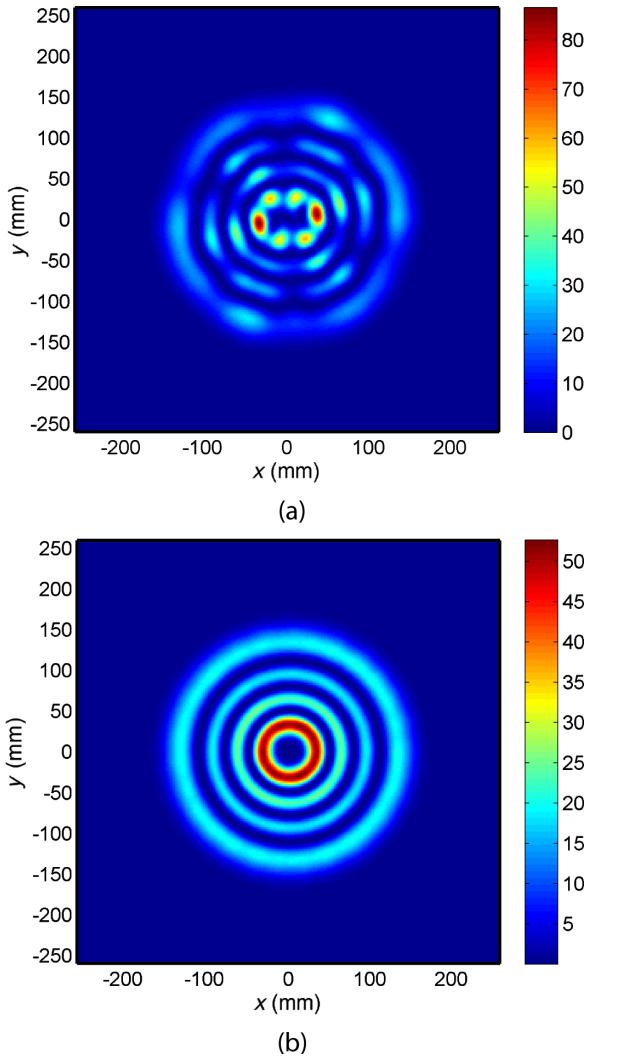

FIG. 14 (color online). Intensity distribution of beam reflected from simulated arm cavity. (a) Using original mirror maps. 79.0% in the LG33 mode (b) Using corrected mirror maps. More than 99.9% in the LG33 mode. Color scale in W/m^2.

interferometer, as this performance is equivalent to that of the HG00 fundamental mode using the original mirror maps (99.97%).

VII. CONCLUSION

In this article we discussed the problem of imperfect intra-cavity mirrors scattering light into higher order modes that are on or near resonance. In the case of second generation GW interferometers this results in an increase in round-trip losses and slight deterioration in contrast defect on the dark port together with potential instabilities in alignment signals. In the case of using LG33 modes in third generation interferometers this results in an unacceptable contrast defect due to the higher order mode content in the reflected field which can be as high as 20%. The logical solution is to improve mirror polishing technology and metrology. However achieving sub-angstrom polishing on such large optics is a daunting task. We therefore proposed an alternative technique whereby we selectively correct *in situ* the surface figure of the cavity mirror, thereby minimizing the scattering from the desired mode into other modes that may be on or close to resonance. We present an algorithm that allows us to determine and remove specific features of a mirror map that generate this unwanted scattering.

We present the example of the AdV Virgo arm cavity whereby we correct mirror maps such as to suppress scattering into the 8th and 9th higher order modes. Optical simulations with the corrected mirror maps resulted in a reduction of more than a factor 20 in 8th and 9th higher order mode content in the reflected field, together with a reduction of 40% in the cavity round-trip losses. Such improvements would have a notable effect on the Advanced Virgo performance. We then demonstrated that such mirror corrections could be achieved experimentally using central heating residual aberration correction (CHRAC). An array of blackbody emitters projects heat onto the high reflectivity surface of the cavity mirror thereby deforming it thermo-elastically. Simulations showed that, for a maximum emitter temperature of 1200 degrees Celsius, a maximum absorbed intensity of 52 $\mathrm{mW/cm^2}$ could be achieved. The combination of thermal simulations and adaptive optics algorithms were employed to determine the heater array pattern needed to apply the required mirror correction. It was found that the desired mirror correction could be achieved by using CHRAC to a high level of accuracy. The total absorbed power was found to be around 600 mW and the peak intensity absorbed was 7 $\mathrm{mW/cm^2}$ which is just one seventh of the actuator's dynamic range.

We used the same approach for the application of LG33 modes. We determined correction maps which suppress scattering from the LG33 modes into other 9th order modes. Such a correction resulted in the LG33 mode content in the reflected beam increasing from 79.0% to more than 99.9% which would result in an acceptable contrast defect at the dark port.

In order to have a complete practical solution it will be necessary to have an adequate sensing and control system. Preliminary studies have shown that this should be feasible and work concerning this subject will be published in a subsequent article.

It will take many years for polishing and metrology techniques to achieve the requirements that are being demanded within the GW community. Adaptive optics has been used in many fields in the past few decades to combat aberrations that we are unable to compensate otherwise. It therefore appears to be a natural development to use a device such as CHRAC in an adaptive optics system in GW interferometers in order to obtain a performance that could not be otherwise achieved.

ACKNOWLEDGMENTS

The research activity of one of the authors (G. V.) has been partially supported by Regione Toscana (Italy) through the program POR CreO FSE 2007-2013 of the European Community, within the Project No. 18113 (ISAV). The authors would like to thank F. Bondu for supplying the code to generate the random mirror maps.

[1] B. P. Abbott *et al.*, Rep. Prog. Phys. **72**, 076901 (2009).
[2] T. Accadia *et al.*, J. Instrum. **7**, P03012 (2012).
[3] H. Luck *et al.*, Classical Quantum Gravity **23**, S71 (2006).
[4] D. Tatsumi and the TAMA Collaboration, J. Phys. Conf. Ser. **120**, 032011 (2008).
[5] P. R. Saulson, *Fundamentals of Interferometric Gravitational Wave Detectors* (World Scientific, Singapore, 1994).
[6] W. Winkler, R. Schilling, K. Danzmann, J. Mizuno, A. Rudiger, and K. A. Strain, Appl. Opt. **33**, 7547 (1994).
[7] T. Accadia *et al.*, Classical Quantum Gravity **30**, 055017 (2013).
[8] T. Accadia *et al.*, Report No. VIR-0128A-12, 2012, https://tds.ego-gw.it/ql/?c=8940.
[9] R. Bonnand, G. Cochez, J. Degallaix, R. Flaminio, L. Giacobone, B. Lagrange, F. Marion, C. Michel, B. Mours, P. Mugnier, E. Pacaud, and L. Pinard, Gravitational-Wave Advanced Detector Workshop, Hawaii, 2012 (unpublished), https://dcc.ligo.org/public/0092/G1200630/001/GWADW12_bonnand.pdf.

[10] G. M. Harry, H. Armandula, E. Black, D. R. M. Crooks, G. Cagnoli, J. Hough, P. Murray, S. Reid, S. Rowan, P. Sneddon, M. A. Fejer, R. Route, and S. D. Penn, Appl. Opt. **45**, 1569 (2006).
[11] B. Mours, E. Tournefier, and J.-Y. Vinet, Classical Quantum Gravity **23**, 5777 (2006).
[12] S. Chelkowski, S. Hild, and A. Freise, Phys. Rev. D **79**, 122002 (2009).
[13] T. Hong, J. Miller, H. Yamamoto, Y. Chen, and R. Adhikari, Phys. Rev. D **84**, 102001 (2011).
[14] C. Bond, P. Fulda, L. Carbone, K. Kokeyama, and A. Freise, Phys. Rev. D **84**, 102002 (2011).
[15] B. Sorazu, P. J. Fulda, B. W. Barr, A. S. Bell, C. Bond, L. Carbone, A. Freise, S. Hild, S. H. Huttner, J. Macarthur, and K. A. Strain, Classical Quantum Gravity **30**, 035004 (2013).
[16] R. A. Day, Gravitational-Wave Advanced Detector Workshop, Hawaii, 2012 (unpublished), https://dcc.ligo.org/public/0092/G1200629/001/DAY_GWADW2012.pdf.
[17] M. Kasprzack, B. Canuel, F. Cavalier, R. A. Day, E. Genin, J. Marque, D. Sentenac, and G. Vajente, Appl. Opt. **52**, 2909 (2013).
[18] A. Rocchi, E. Coccia, V. Fafone, V. Malvezzi, Y. Minenkov, and L. Sperandio, J. Phys. Conf. Ser. **363**, 012016 (2012).
[19] M. Evans, S. Ballmer, M. Fejer, P. Fritschel, G. Harry, and G. Ogin, Phys. Rev. D **78**, 102003 (2008).
[20] M. A. Vorontsov and G. W. Carhart, J. Opt. Soc. Am. A **17**, 1440 (2000).
[21] M. A. Vorontsov and V. P. Sivokon, J. Opt. Soc. Am. A **15**, 2745 (1998).